Experimental verification of a novel hierarchical lattice material with superior buckling strength

Bluhm, Gore Lukas; Christensen, Keld; Poulios, Konstantinos; Sigmund, Ole; Wang, Fengwen

Published in:
APL Materials

Link to article, DOI:
10.1063/5.0101390

Publication date:
2022

Document Version
Publisher's PDF, also known as Version of record

Experimental verification of a novel hierarchical lattice material with superior buckling strength

Cite as: APL Mater. 10, 090701 (2022); doi: 10.1063/5.0101390
Submitted: 31 May 2022 • Accepted: 19 August 2022 •
Published Online: 14 September 2022

Gore Lukas Bluhm,[a] Keld Christensen, Konstantinos Poulios, Ole Sigmund, and Fengwen Wang

AFFILIATIONS

Department of Civil and Mechanical Engineering, Technical University of Denmark, Nils Koppels Allé, Building 404, 2800 Kgs. Lyngby, Denmark

Note: This paper is part of the Special Topic on Design, Material, Function, and Fabrication of Metamaterials.
[a]**Author to whom correspondence should be addressed:** glubluh@dtu.dk

ABSTRACT

Recently, a systematic approach for the design of lattice materials with extreme buckling strength has led to optimized hierarchical lattice materials with unprecedented load carrying capacity. This is obtained at the cost of a small decrease in linear stiffness. However, the superior buckling resistance of such optimized hierarchical lattice materials has so far only been predicted numerically. In fact, concerns have been raised regarding the validity of the employed linear buckling analysis and potential risk of catastrophic failure due to the coalescence of multiple critical buckling modes. This work aims at refuting these concerns by designing and testing manufacturable novel hierarchical lattice materials with superior buckling strength. Thereby, the basis is provided for wide applications of these high-performing materials in mechanical design. A novel hierarchical material is generated for this work by combining the mentioned design procedure with a requirement on the minimum feature size to ensure manufacturability. For addressing the raised concerns, the optimized material design, together with a reference material, is realized with the help of additive manufacturing and experimentally tested in uniaxial compression. The obtained results are compared to numerical simulations considering geometrical and material nonlinearities, and an overall good agreement is found between experimental and numerical results. This confirms an increase in buckling resistance and post-buckling load carrying capacity by a factor of more than three compared to the regular reference lattice structure. Hence, the buckling superiority of this novel type of architected materials is clearly demonstrated.

I. INTRODUCTION

Architected periodic materials have been extensively studied and developed for numerous applications due to their favorable and tunable material properties. Within the scope of mechanical properties, examples have, among others, been shown for programmable and optimal linear elastic properties,[1–6] energy absorption,[7–9] resilience of hierarchical materials,[10–12] auxetic behavior,[13–16] and desired nonlinear load–displacement relations.[17–19]

Recently, 2D periodic materials have been systematically designed for enhanced buckling resistance using topology optimization based on linear buckling analysis and Floquet–Bloch wave theory, as initially introduced by Neves *et al.*[20] and much refined by Thomsen *et al.*[21] In this approach, the unit cell is optimized in an iterative procedure. For every optimization iteration, the strength of the current design is evaluated using linear finite element buckling analysis together with Floquet–Bloch boundary conditions to capture all possible buckling modes. By sweeping over the wavevectors $\boldsymbol{k}$ along representative lines of the irreducible Brillouin zone, the buckling band diagram is obtained and the material buckling strength is determined by the smallest buckling factor in the band diagram. Subsequently, the material distribution is updated based on gradient information to maximize the strength of the design. This results in a material design, which is resistant to buckling across all wavelengths. For illustration, Fig. 1 shows the material buckling evaluation of two lattice materials considered in this study.

In the work of Thomsen *et al.*,[21] it was numerically predicted that the buckling strength can be significantly improved at the cost of a comparably small stiffness degradation by the resulting hierarchical microstructure. However, concerns were expressed about the validity of the employed linear buckling theory and the danger of

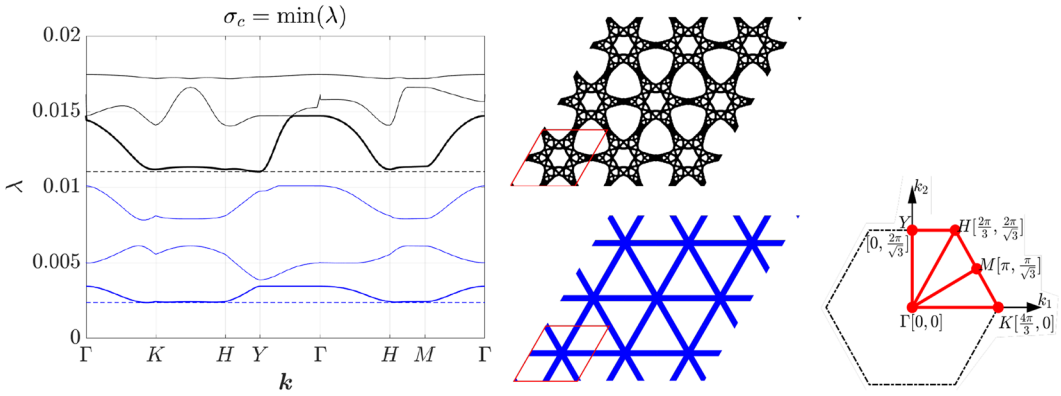

(a) Band diagram (b) Lattice materials (c) Brillouin zone

FIG. 1. Linear material buckling evaluation (a) including the three lowest buckling modes along the symmetry lines of the first irreducible Brillouin zone (c) for the regular and hierarchical lattice materials (b). $\boldsymbol{k}$ represents the wavevector and λ is the buckling stress, normalized by Young's modulus of the base material (E). Experimental results in Fig. 9 are related by $\sigma_c = F/(LTE)$. The periodic unit cells are highlighted by the red rhombus.

catastrophic failure and unpredictable post-buckling deformations due to multiple critical or near-critical buckling modes, spanning over a large range of wavelengths. This phenomenon is illustrated by the buckling band diagram in Fig. 1 exemplarily showing the three lowest buckling modes of an infinite periodic reference triangular material structure as well as the corresponding optimized hierarchical microstructure. Besides the significantly enhanced buckling resistance of the hierarchical lattice, the curves representing the critical modes show flat plateaus along $K - M - H - Y$ lines, indicating simultaneous buckling modes with multiple different wavelengths and orientations. As speculated above, such behavior may introduce unpredictable and catastrophic post-buckling response for realized finite structures.

In the following years, these issues were numerically addressed by Bluhm *et al.*[22] and Wang and Sigmund[23] by nonlinear analyses of a representative hierarchical square lattice from the work of Thomsen *et al.*,[21] where the buckling and post-buckling performances of the hierarchical lattices were compared against a corresponding regular lattice. However, experimental confirmations and accurate physical modeling of the constituent materials have been lacking.

For the first time, physical specimens of hierarchical lattices systematically optimized for buckling resistance are manufactured and evaluated experimentally under uniaxial compression. A realizable design of an initially isotropic, hierarchical triangular lattice is obtained by combining the material design method of Thomsen *et al.*[21] with a minimum length scale control to ensure manufacturability using a single-case robust formulation as in Ref. 6. In addition to the experimental testing of the optimized hierarchical lattice, the regular 2D periodic triangular lattice is tested to provide a baseline at a theoretical volume fraction of 0.3.

The experimental evaluation is complemented by a series of nonlinear finite element analyses, based on the 3D geometry of the tested specimens. In contrast to previous numerical analyses of an orthotropic hierarchical square lattice material,[22,23] the numerical results of this work account for the specific, finite number of unit cells in the physical specimens. Also, a more specific material model fitted to the actually tested material and 3D effects are included. In order to facilitate direct comparisons with earlier studies, numerical and experimental results for the orthotropic square unit cell materials, both regular and optimized (for equi-biaxial loading), are provided in the Appendix.

II. METHODS

A. Design and manufacturing of test specimens

In the material optimization procedure presented by Thomsen *et al.*,[21] a minimum length scale was intrinsically imposed due to the discretization and filtering. Nevertheless, some of the obtained designs include very fine features that challenge the manufacturing and structural integrity of a corresponding mold. In order to ensure manufacturability, a new design has been generated specifically for the present work by extending the buckling optimization with a minimum length scale control using a single-case robust formulation.[24] This results in a minimum feature size, both in the solid structure and the enclosed holes of ~0.02 times the unit cell width. The material usage was constrained to a volume fraction (V^*) of 0.3. The optimized material design for uniaxial compression and the corresponding linear material buckling evaluation are presented in Fig. 1, also including a comparison to a regular reference lattice material. Photographs of the actual specimens of both the optimized hierarchical microstructure and the regular counterpart are shown in Fig. 2.

In order to prevent any material failure prior to buckling, the test specimens for the experiments were made of silicone rubber, a material that allows for the required large elastic deformations. The complex geometries were realized in a hybrid process by casting the specimens using 3D-printed molds of PLA (polylactic acid). As an example, Fig. 3 shows the lower and upper parts of the mold, manufactured in an FDM (fused deposition modeling) printer, for the hierarchical triangular lattice material. Since the aim is to obtain a perfect extrusion of the 2D material design, all molds were designed with no taper angle. For this reason, the molds had to be

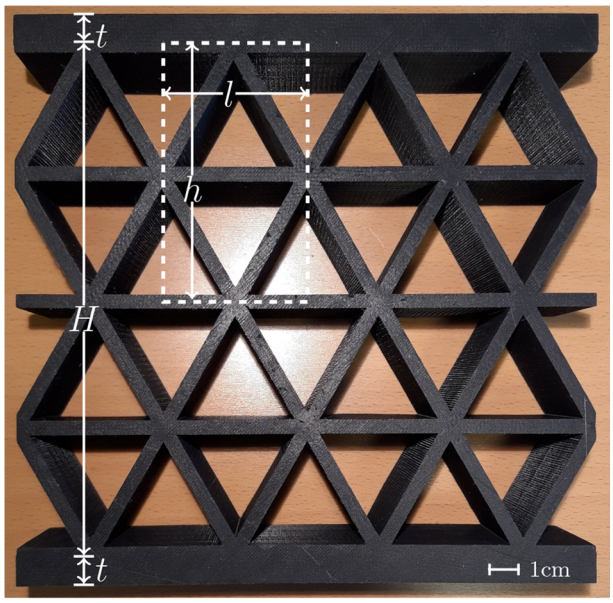

(a)

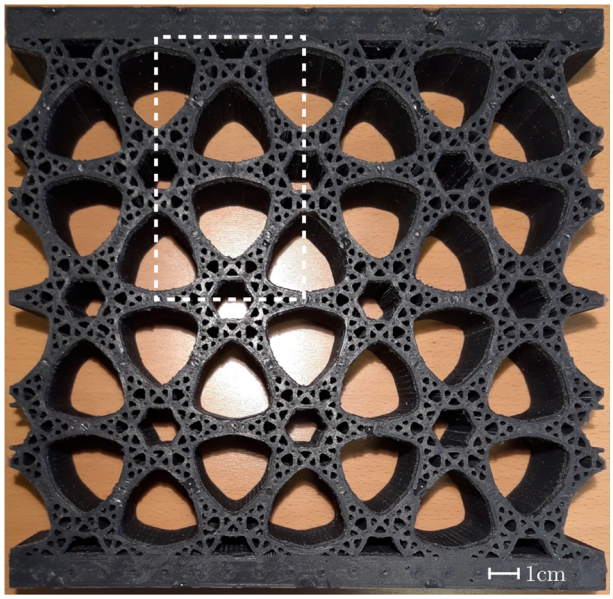

(b)

FIG. 2. Photographs of the investigated specimens. The dashed boxes indicate the unit cells. (a) Regular triangular lattice (4 × 2 unit cells). (b) Hierarchical triangular lattice (4 × 2 unit cells).

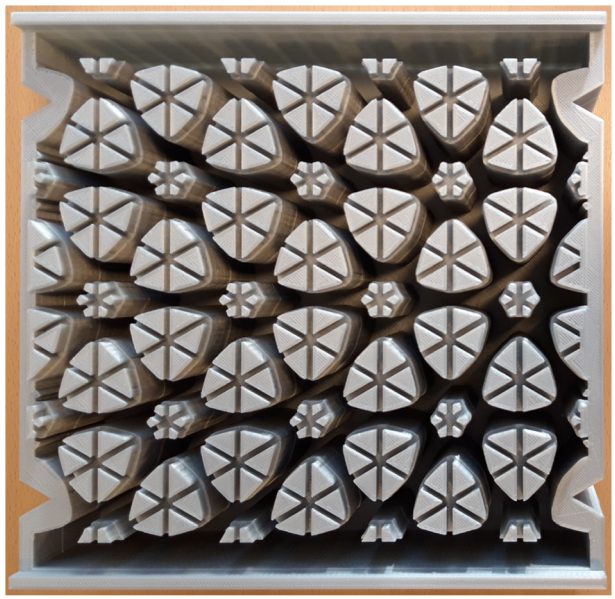

(a)

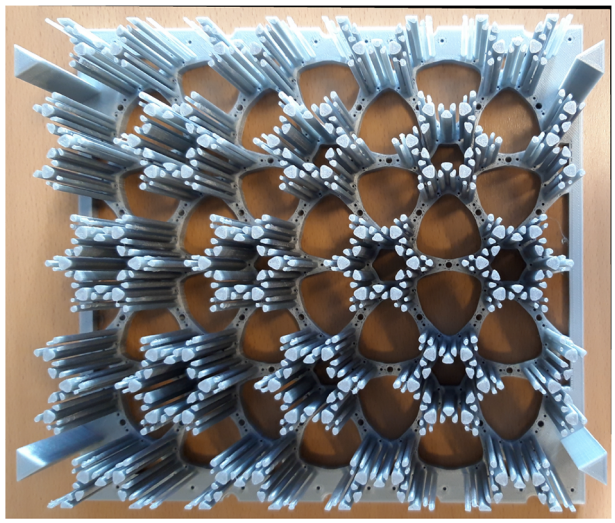

(b)

FIG. 3. 3D-printed mold for the hierarchical triangular lattice material. (a) Lower part of the mold. (b) Upper part of the mold.

removed destructively from the specimens after the material was solidified. Total dimensions, number of unit cells in the specimen, and minimum feature size are limited by the printing area and the required precision for the 3D-printed molds. These restrictions led to the choice of specimens composed of 4 × 2 unit cells (rectangular representation) with a height of $h = 82$ mm and a width of $l = h\tan(30^\circ) \approx 47.34$ mm. In order to support the lattice structure and distribute the applied load, solid blocks with a height of 10 mm were added both at the top and the bottom of the specimens. To avoid out-of-plane buckling during the experiments, a relatively large thickness of $T = 45$ mm was chosen for the specimens.

For the hierarchical specimen, the 3D printed lower part of the mold was filled with a condensation cure silicon rubber compound and then closed with the upper half of the mold. The filled mold was shaken and knocked against a tabletop to help

trapped air bubbles from the mixing procedure to escape before the silicone rubber solidified. The cast was left to cure for at least 24 h before removing it from the mold. Especially for the two hierarchical lattice specimens, removal of the mold was only possible with breaking some of their thin members; hence, these molds were not reusable.

The cast specimens turned out to be of good quality based on visual inspections, as shown in Fig. 2. The specimens were weighed, and their real volume was estimated based on a specific mass of 1.1 g/cm^3 for the base material. The regular lattice specimen was very close to the nominal volume fraction of 0.3. In contrast, the hierarchical lattice specimen exhibited a weight that corresponds to a volume fraction of ~0.33 rather than 0.3 due to manufacturing errors in the complex mold for the hierarchical case. In order to compensate for this discrepancy, the geometry of the hierarchical structure used in the numerical analysis was also dilated uniformly to match the estimated volume fraction of 0.33. Simulation results for a dilated specimen of the regular lattice at $V^* = 0.33$ are included as well for comparisons.

B. Experimental setup

The specimens were tested under uniaxial compression. For this purpose, they were placed between lower and upper rigid plates mounted on an electromechanical MTS test machine, and the experiment was performed in displacement control mode. Friction between the plates and the specimens prevented sliding perpendicular to the loading direction. No further fixation of the specimens or guidance in the out-of-plane direction was enforced. The relatively large thickness of the specimens (45 mm) was sufficient to ensure that in-plane buckling modes of the structures are the critical ones.

The uniaxial testing machine was equipped with a load cell with a nominal maximum capacity of 1 kN. The displacement controlled compression was performed with a constant rate of 5 mm/min for all tests. This low rate was chosen in order to minimize the influence of rate dependent viscous effects of the silicone rubber material. Multiple experimental runs were carried out on a single specimen for each of the different lattice materials.

C. Nonlinear numerical analysis

Preliminary comparisons between a plane strain, a plane stress, and a 3D model for one of the specimens revealed that none of the two 2D simplifications can reproduce the force-displacement response of the 3D geometry satisfactorily as shown in Fig. 4. In the pre-buckling regime, the plane stress model slightly underestimates the reaction force, while the plane strain model overestimates it significantly for the same compression. Also, both 2D simulations underestimate the buckling strain and the remaining post-buckling stiffness. The invalidity of both 2D assumptions is related to the significant thickness, compared to the in-plane feature size, as well as the non-uniform stress states. Based on these observations, all numerical analyses were carried out using 3D models to ensure comparability with the experimental tests.

To mitigate the higher computational cost of the 3D models, symmetry in the out-of-plane direction was exploited, and thereby, only half of each specimen geometry was modeled. Each structure was sliced at the half thickness plane, as illustrated in Fig. 5 for the regular lattice, with the slicing plane highlighted in green. Symmetry was imposed by prescribing zero z-displacements on the symmetry plane.

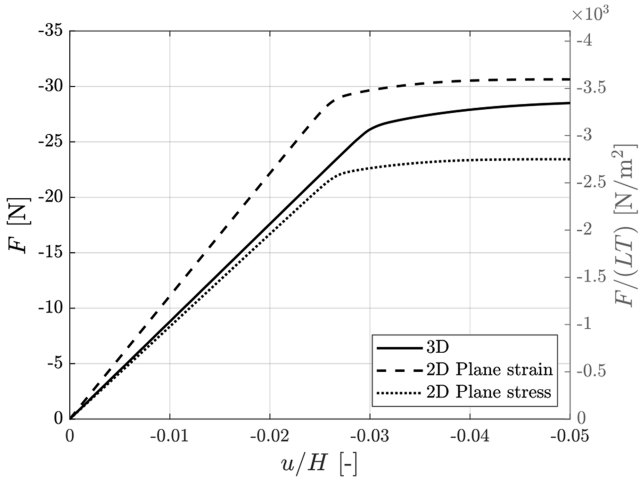

FIG. 4. Load–displacement curves for the regular lattice based on a 3D model and 2D simulations.

Perfectly sticking boundary conditions were assumed at the top and bottom interfaces between the specimen and the rigid plates mounted to the test machine. Accordingly, both y- and z-displacements at the relevant faces were fixed. At the bottom face, colored blue in Fig. 5, the displacements in the x-direction were fixed as well. At the top face, colored red in Fig. 5, a prescribed x-displacement was imposed on all finite element nodes. The prescribed displacement value, in the following referred to simply as u, was incremented in several quasi-static load steps in order to simulate the experimental procedure.

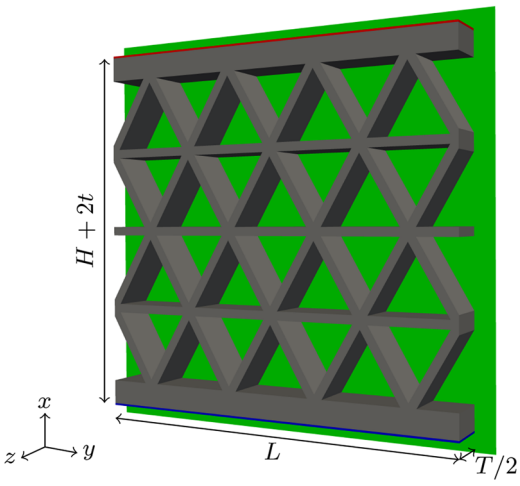

FIG. 5. Schematic of the 3D model. Symmetry plane shown in green ($u_z = 0$), fully fixed boundary in blue ($u_x = u_y = u_z = 0$), and compression boundary in red ($u_y = u_z = 0, u_x \neq 0$).

The regular lattice specimen was discretized with 27-node hexahedral elements, while the hierarchical specimen was discretized with a mixture of 18-node prisms for the internal unit cells and 27-node hexahedrons for the supporting structure at the top and bottom. Each internal strut in the regular lattice was discretized with eight second-order elements across its in-plane thickness. The in-plane mesh used for the hierarchical structure is shown in Fig. 6. In the out-of-plane direction z, all structures were modeled with three second-order elements spanning the half-thickness $T/2$. This means effectively six elements for the entire thickness if symmetry was not exploited. Furthermore, a variable element size was used in the z-direction with smaller elements close to the free front surface of the structure. The non-uniformly spaced node coordinates between elements are at $z = 0, 10, 17.5,$ and 22.5 mm, with the symmetry plane located at $z = 0$ mm.

The silicone rubber material was modeled using the hyperelastic Mooney–Rivlin material law[25] in compressible form with the following strain energy density function:

$$W = \frac{K}{2}(J-1)^2 + C_{10}\left(\bar{I}_1 - 3\right) + C_{01}\left(\bar{I}_2 - 3\right), \tag{1}$$

where $J = |\boldsymbol{F}|$ is the determinant of the deformation gradient, and $\bar{I}_1 = \mathrm{tr}\left(\bar{\boldsymbol{B}}\right)$ and $\bar{I}_2 = \frac{1}{2}\left(\mathrm{tr}\left(\bar{\boldsymbol{B}}\right)^2 - \mathrm{tr}\left(\bar{\boldsymbol{B}}^2\right)\right)$ are the first and second invariants of the isochoric part $\bar{\boldsymbol{B}} = J^{-2/3}\boldsymbol{F}^T\boldsymbol{F}$ of the left Cauchy–Green strain tensor. The bulk modulus is denoted K, and C_{10} and C_{01} are material coefficients of the Mooney–Rivlin material. These material properties were determined experimentally as described in Sec. II D.

The numerical model was implemented using the finite element library GetFEM[26] and meshes were generated using GMSH.[27] For capturing relevant buckling modes in the nonlinear analysis, the otherwise geometrically perfect structures need to be perturbed appropriately. In this work, random geometric perturbations covering multiple length scales were applied based on the method presented in Bluhm *et al.*[22] This ensures a level of continuity in the otherwise random perturbation. For every length scale, a 2D grid of control points is defined on top of the in-plane geometry of the given specimen, equally spaced according to the length scale. Each control point is assigned a random perturbation, and the nodes in the actual mesh are displaced using linear interpolation between the surrounding control points. The magnitude for the control points at the interface to the supporting material is set to zero for maintaining parallel and aligned faces at the top and bottom. The final perturbation of the mesh is given by the superposition of the perturbation at every length scale with the maximum magnitude of every individual contribution scaled relative to the length scale. This concept is illustrated in Fig. 7 showing an exemplary perturbation magnitude of three grids with different length scales.

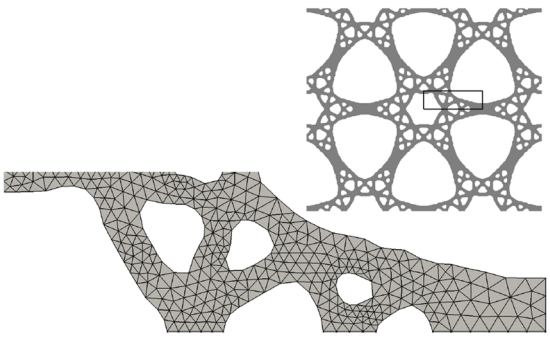

FIG. 6. Front view of a representative cutout of the mesh for the hierarchical material.

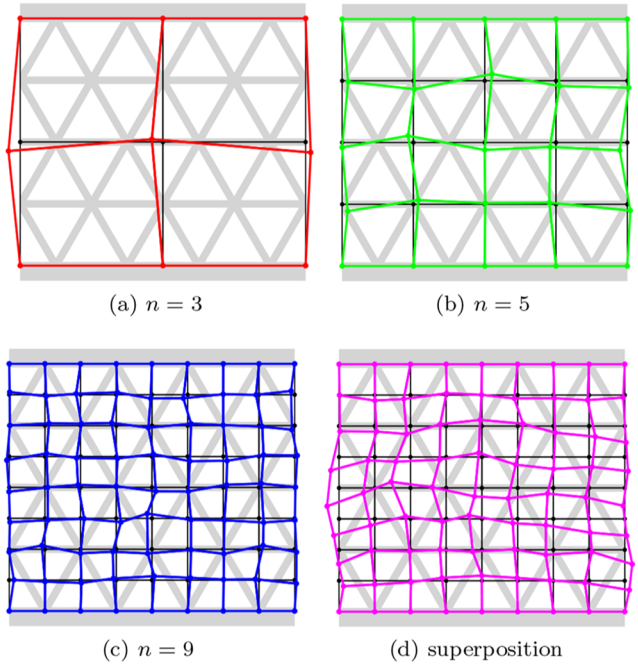

FIG. 7. Exaggerated perturbation fields for control point grids with different length scales given by the number of control points n in both directions (a)–(c) and the total perturbation (d). Length scales, relative to the specimen size, are related to the number of control points by $1/(n-1)$. The magnitudes are scaled by a factor of 10 compared to the ones used in this work.

Including several length scales is especially important for multiscale structures in order to facilitate buckling modes at different levels in the hierarchy of the structure. The following results are based on stochastic perturbations imposed on three length scales of 1/2, 1/4, and 1/8 of the total dimension. The theoretical maximum amplitude is $0.04l$, where l is the unit cell length. This value can only be reached if all random values assigned to the control grids take their maximum value at a specific point.

D. Material properties

In order to determine the material properties of the silicone rubber for the numerical analysis, a uniaxial compression test of a solid cube with a side length of 30 mm was performed. From manual model calibration using a 3D finite element analysis of the same cube, a set of parameters was obtained. Based on the strain energy density function [Eq. (1)], a well-suited set of parameters that captures both the initial stiffness and the characteristic stiffening at higher compression was found as $K = 7.407$ MPa,

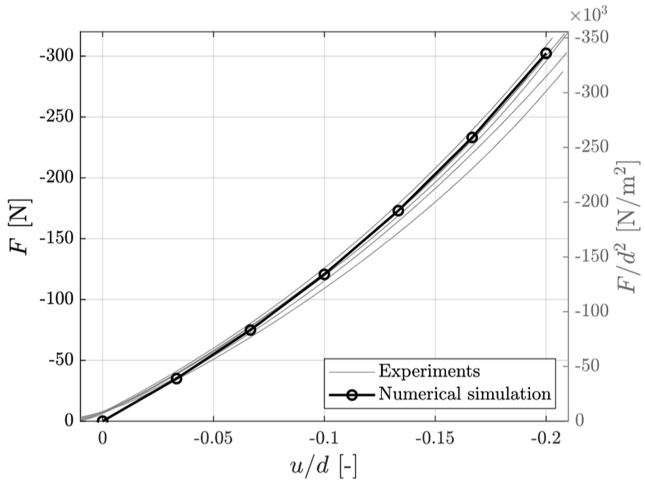

FIG. 8. Load–displacement response of a solid material cube (side length d = 30 mm) under uniaxial compression.

C_{10} = 0.030 03 MPa, and C_{01} = 0.1201 MPa. These parameters correspond to an initial shear modulus $G = 2(C_{10} + C_{01})$ = 0.3003 MPa and an initial Poisson's ratio ν = 0.48. The measured load responses as a function of the normalized compression displacement for multiple experimental runs on the same specimen are shown in Fig. 8. In addition, the figure presents the simulation results for the estimated material properties.

III. RESULTS AND DISCUSSION

Figure 9 shows load–displacement curves from both numerical simulations and experiments for the investigated specimens. The nonlinear analysis of the regular specimen at the nominal volume fraction (red dashed line) shows a good agreement with the experimental data, represented by the thinner solid lines. The pre-buckling stiffness is predicted accurately, while the post-buckling response is slightly more compliant compared to the experimental data, and the buckling load is overestimated by 9%. Figure 10 illustrates the structural deformations at different compression levels from the experiments and nonlinear analysis. It can be seen that the predicted buckling mode is the same as experimentally obtained. This shows the capability of the numerical model to describe the behavior of the triangular periodic lattice specimen accurately. Based on this validation, simulations of the same, but uniformly dilated geometry, are included in the figure as well (blue dashed line) in order to provide a fair comparison to the slightly heavier realization of the hierarchical microstructure. As expected, the initial stiffness of the dilated geometry with V^* = 0.33 is increased by ~10%, in accordance with the change in volume fraction. However, the buckling load is increased significantly more, as the bending stiffness is proportional to the cube of the in-plane-thickness, according to linear theory.

Results for the critical buckling from a linear buckling analysis of the same finite 3D geometries are included in Fig. 9 as gray crosses. When compared to the nonlinear simulations, they are ~10% lower for both regular lattices. The experimentally obtained buckling point was predicted well by the linear buckling estimate for the case of 0.3 volume fraction. For the hierarchical structure, linear analysis underestimates the buckling limit significantly by 23%, which is noteworthy. The importance of nonlinearities, such as beam thickening,[28] for the optimized hierarchical structures was already recognized in Ref. 22, but now it is also validated experimentally.

A linear buckling 3D analysis of the specimen with optimized structure at 0.33 volume fraction suggests that the hierarchical structure should buckle at almost three times the buckling load

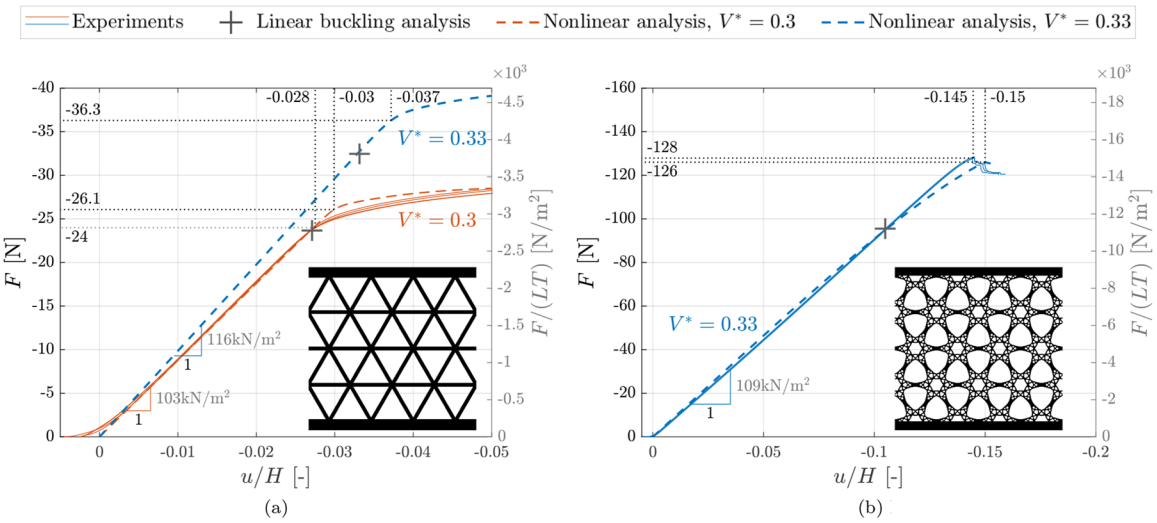

FIG. 9. Load–displacement curves for the considered lattice structures. The right axis shows the corresponding stress, allowing for comparisons with specimens of different dimensions. Buckling is identified as the point of maximum curvature along the load–displacement paths. Note the different scaling of the axes. (a) Regular triangular lattice structure. (b) Hierarchical triangular lattice structure.

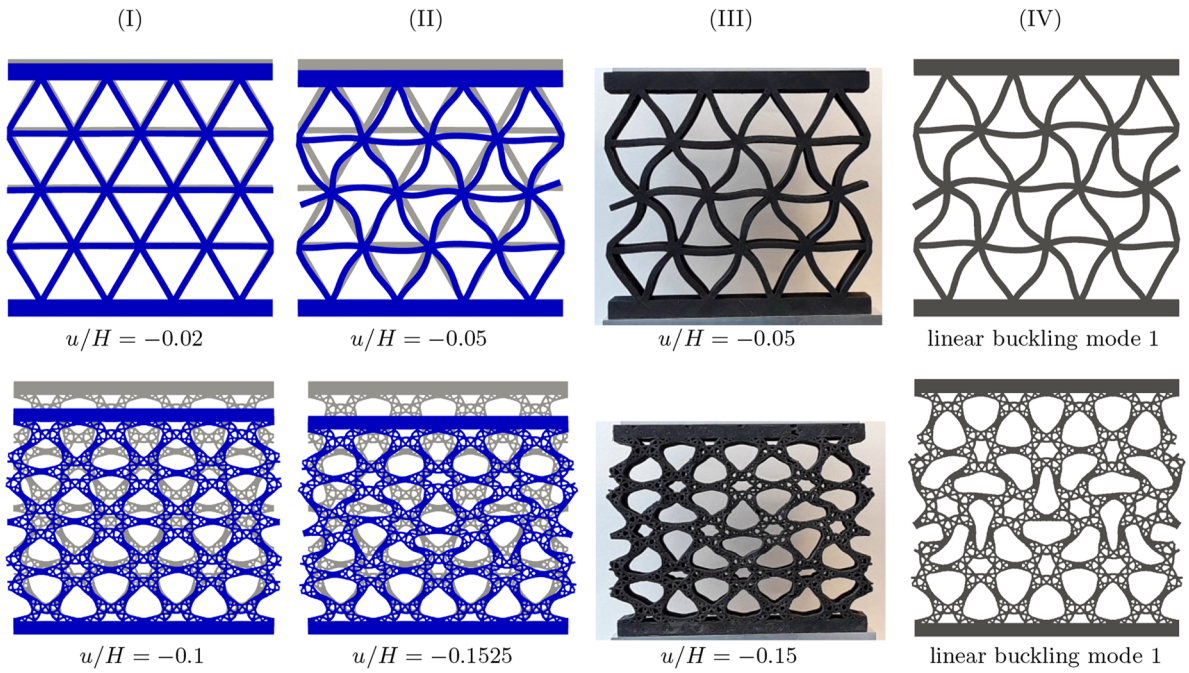

FIG. 10. Numerically obtained lattice deformations at moderate compression (I) and post-buckling state (II), pictures of post-buckling state from the experiment (III), and buckling modes from the linear analysis (IV).

of the corresponding volume-corrected regular lattice (gray crosses in Fig. 9). According to the nonlinear simulations of the same structures, the hierarchical structure is 3.5 times stronger than the regular lattice. Also, buckling of the hierarchical structure occurs at a much larger strain level, 15% instead of 3.7% for the regular lattice. Keeping in mind that the nonlinear simulation tended to overestimate the strength of the regular lattice, this increase in the buckling strength is a conservative estimate and still remarkable. In general, both experimental results and numerical simulations validate the superior load carrying capacity of the optimized hierarchical structure.

For the optimized hierarchical structure, the nonlinear numerical analysis exhibits a slightly higher stiffness in the initial pre-buckling phase compared to the experimental results. For further compression, the structure shows a softening behavior in the numerically obtained load–displacement curve, which is not present in the experimental results. Ultimately, both methods show very similar buckling limits, with less than 2% relative error.

Apart from the mentioned deviations, it is remarkable that the nonlinear numerical analyses can actually reproduce the experimentally observed buckling modes as precisely as shown in Fig. 10 only based on random perturbations of the geometry. From the deformed structures shown in Fig. 10 at different loading states, it is evident that the numerical simulations predict the same post-buckling deformations as obtained experimentally. Both specimens undergo local buckling with conceptually different buckling patterns, which, however, share some local similarities between the hierarchical and regular variants. It should also be noted that the buckling modes predicted by the linear buckling analysis also match well with the experimentally observed post-buckling deformations, as shown in Fig. 10.

In defiance of the anticipated unpredictable post-failure behavior of such hierarchical material designs, the tested hierarchical specimen maintains a load carrying capacity, which even after buckling still is a multiple of the buckling limit of the regular lattices. The measured reaction force drops for the hierarchical structure just after the point of buckling. Nevertheless, the drop in load carrying capacity of the hierarchical lattice is rather small compared to the large strength gain compared to the regular lattices. The experimentally tested hierarchical structure could after buckling sustain a load of 120 N, which still is more than three times larger than the load sustained by the regular triangular lattice with the same volume fraction ($V^* = 0.33$). This result addresses the posed question about the possibility of a catastrophic buckling. Despite the slight drop in load at the buckling point, the structure has a remarkably high load carrying capacity even in the post-buckling state. Moreover, buckling occurs for the hierarchical structure at such high deformation levels that internal contact between the structure's finest members is imminent. Shortly after buckling, an additional strengthening can be expected due to internal contact. In total, a catastrophic collapse does not turn out to be a concern for the optimized hierarchical structure of this study, suggesting that these structures are excellent candidates for manufacturing high strength architected materials, especially with base materials that can undergo large strains, such as elastomers.

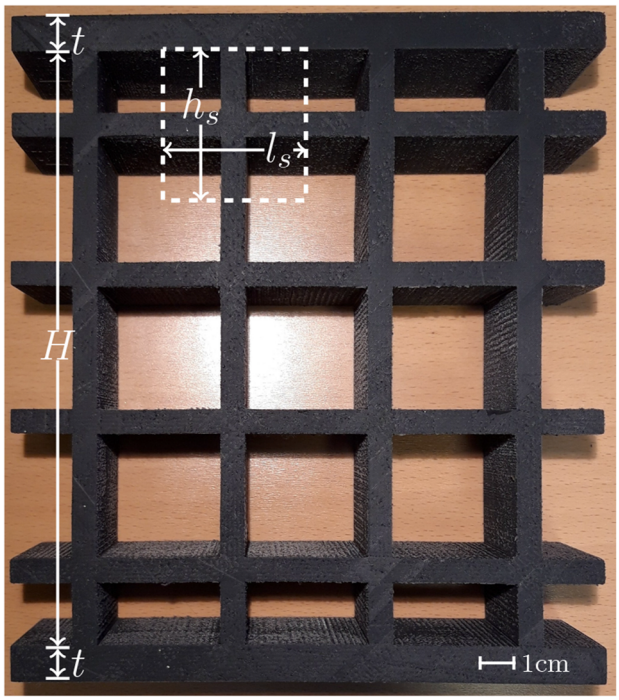

(a)

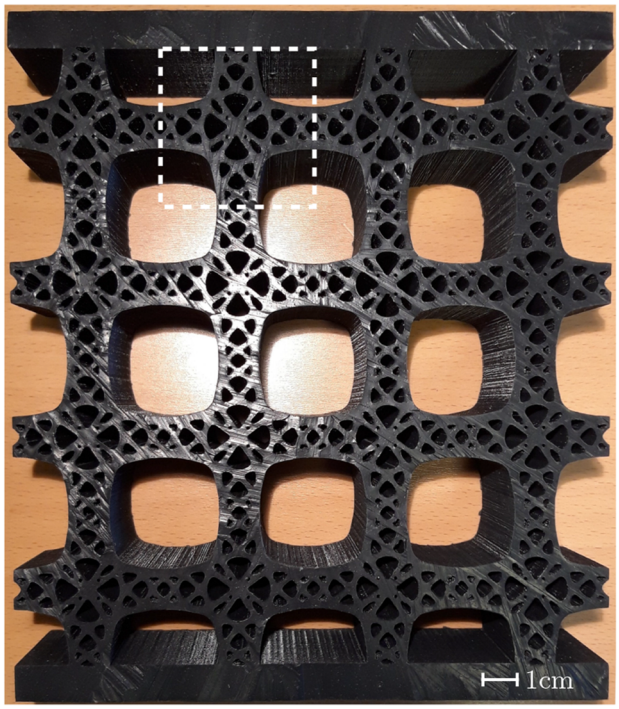

(b)

FIG. 11. Photographs of the investigated specimens. The dashed boxes indicate the unit cells. (a) Regular square lattice (4 × 4 unit cells). (b) Hierarchical square lattice (4 × 4 unit cells).

IV. CONCLUSIONS

Experimental testing and nonlinear numerical 3D simulations were performed in order to evaluate the performance of an optimized hierarchical lattice material, designed by density-based topology optimization,[21] compared to a corresponding regular lattice of a similar volume fraction. Although the hierarchical lattice was optimized for plane stress conditions using linear buckling theory, and for an infinite periodic material, it proved to perform excellently, in terms of compressive load capacity, in a real 3D structure with a finite number of unit cells and with nonlinearities included. In fact, due to nonlinear effects, the attained load carrying capacity for the structures was found to be 30% higher than the linear buckling limit estimate.

The nonlinear numerical analyses match the experiments reasonably well with an error of less than 10%. They are capable of predicting the experimentally observed buckling modes remarkably accurately both for regular and hierarchical lattices. Predicted buckling strains were only slightly overestimated and the same applies to predicted buckling loads for the regular lattice. The critical load for the hierarchical lattice is predicted very accurately.

It should be noted that due to manufacturing inaccuracies, the hierarchical lattice structure had a slightly higher volume fraction of 0.33 instead of 0.3 for the regular one. This is compensated by providing numerical results for a dilated version of the regular lattice, leaving no doubt about the superior buckling strength of the hierarchical lattices compared to their regular counterparts. The load carrying capacity is higher by a factor of ~3.5.

Overall, this work has demonstrated the following:

- Hierarchical architected materials, obtained with topology optimization, linear buckling, and Floquet–Bloch theory in 2D, are realizable and actually deliver the expected outstanding compressive strength.
- The hierarchical lattice structure, unlike the regular one, exhibits a notable additional strengthening effect due to

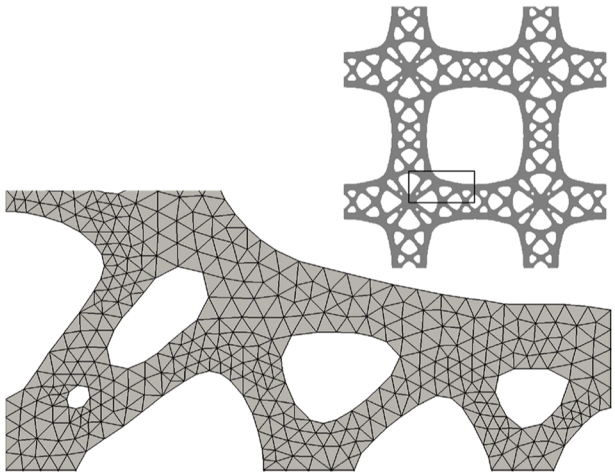

FIG. 12. Front view of a representative cutout of the mesh for the hierarchical square lattice specimen.

nonlinearities, and the gain is thereby even larger than predicted by linear buckling theory.
- The post-buckling load carrying capacity of the hierarchical material remains at a significantly higher level compared to the regular lattice, despite the discussed clustering of critical buckling modes.
- Three-dimensional modeling is required to accurately predict the experimental response of the specimens in the present setup, as neither plane strain nor plane stress assumptions have proven to be valid.
- Nonlinear finite element modeling is essential for improving the accuracy of the numerical analysis, especially for hierarchical structures.

ACKNOWLEDGMENTS

This work was supported by the Villum Fonden through the Villum investigator project InnoTop and the Independent Research Fund Denmark (DFF) through the TopCon Project (Grant No. 032-00228B). The authors also acknowledge the CELCORR Research Group from DTU-MEK for granting access to the uniaxial test equipment and the Fablab at DTU Construct for providing the 3D printing facilities.

AUTHOR DECLARATIONS

Conflict of Interest

The authors have no conflicts to disclose.

Author Contributions

Gore Lukas Bluhm: Formal analysis (equal); Investigation (equal); Writing – original draft (equal); Writing – review & editing (equal). **Keld Christensen**: Conceptualization (equal); Methodology (equal). **Konstantinos Poulios**: Methodology (equal); Supervision (equal); Writing – review & editing (equal). **Ole Sigmund**: Funding acquisition (equal); Methodology (equal); Supervision (equal); Writing – review & editing (equal). **Fengwen Wang**: Methodology (equal); Supervision (equal); Writing – review & editing (equal).

DATA AVAILABILITY

The data that support the findings of this study are available from the corresponding author upon reasonable request.

APPENDIX: RESULTS FOR SQUARE UNIT CELL MATERIALS

This appendix presents equivalent results for a square unit cell hierarchical microstructure, taken directly from the work of Thomsen *et al.*,[21] together with its regular counterpart. In contrast to the uniaxially optimized triangular lattice structure from the main text, it was optimized for an equi-biaxial compressive loading and has been used as a test candidate for numerical studies of hierarchical materials.[22,23] The provided data are aimed to serve as a reference.

The specimens are shown in Fig. 11 and consist of 4×4 unit cells of size $h_s = l_s = 41$ mm, resulting in the same total height as the triangular lattice specimens. Similar to the case of the triangular lattice, an increase in the nominal volume fraction was observed for the hierarchical lattice. Hence, the numerical simulations were performed for the volume fraction of 0.3 and 0.33 for the regular lattice and 0.33 for the hierarchical lattice. The modeling and discretization of the 3D geometries were as described above, and the mesh for the hierarchical specimen is illustrated in Fig. 12.

The results are shown in terms of load–displacement curves in Fig. 13 and deformed structures in Fig. 14. The additional secondary axis shows the reaction load in stress units and serves for better comparison with the shown results of the triangular lattice specimens.

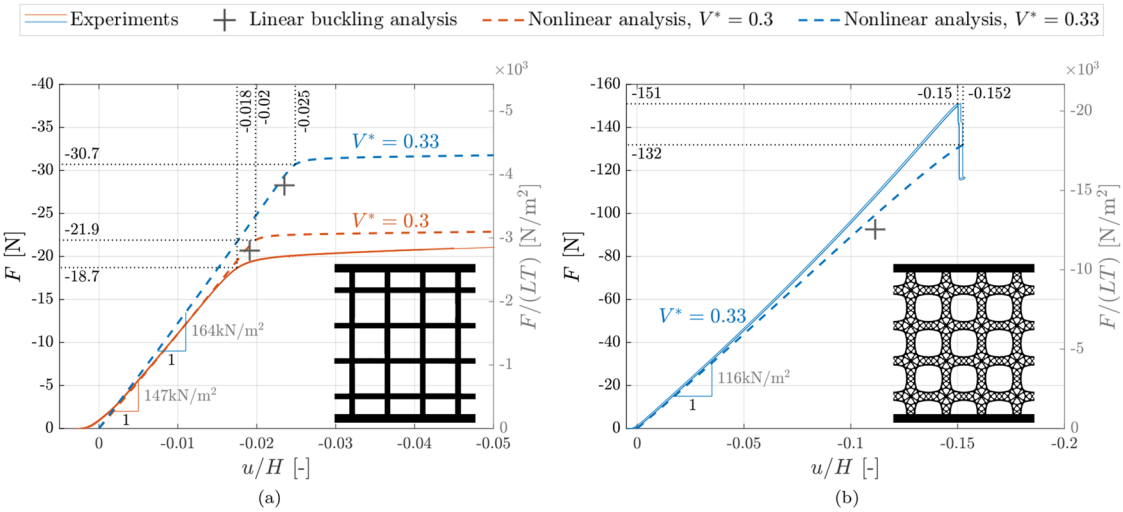

FIG. 13. Load–displacement curves for the square unit cell lattices. Respective lattice microstructures are shown in the figures. (a) Regular square lattice structure. (b) Hierarchical square lattice structure.

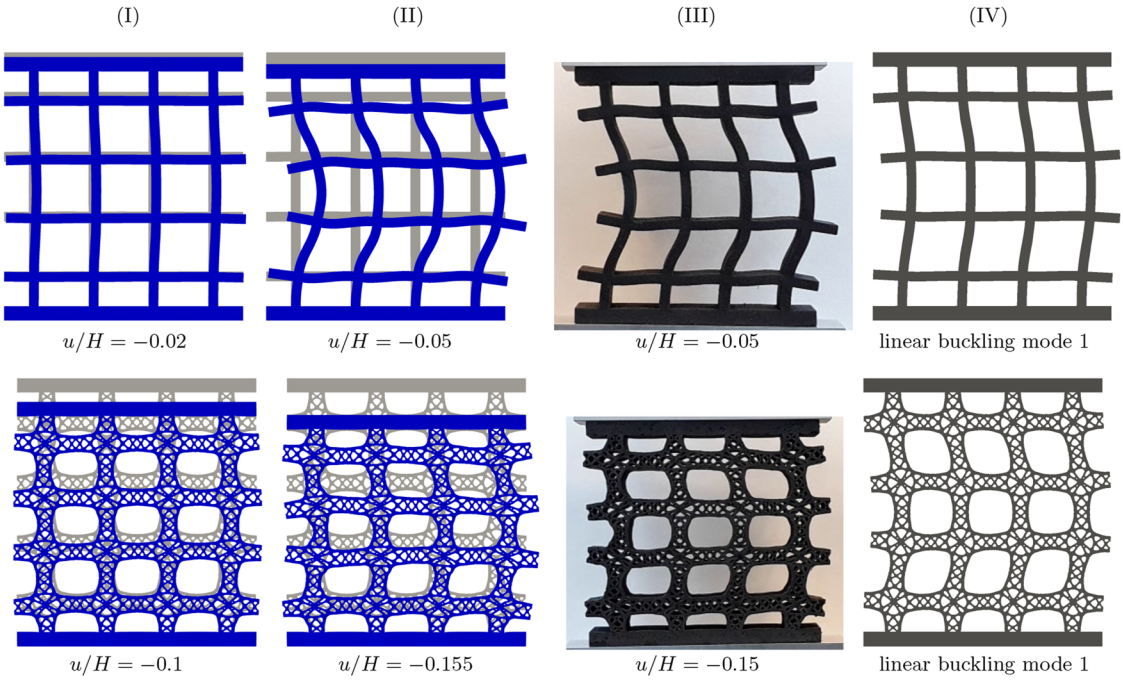

FIG. 14. Numerically obtained lattice deformations at moderate compression (I) and post-buckling state (II), pictures of post-buckling state from the experiment (III), and buckling modes from the linear analysis (IV).

REFERENCES

[1] Z. Hashin, "The elastic moduli of heterogeneous materials," J. Appl. Mech. **29**(1), 143–150 (1962).

[2] O. Sigmund, "Materials with prescribed constitutive parameters: An inverse homogenization problem," Int. J. Solids Struct. **31**(17), 2313–2329 (1994).

[3] O. Sigmund, "Tailoring materials with prescribed elastic properties," Mech. Mater. **20**(4), 351–368 (1995).

[4] M. Ashby, "Hybrid materials to expand the boundaries of material-property space," J. Am. Ceram. Soc. **94**(1), s3–s14 (2011).

[5] J. B. Berger, H. N. G. Wadley, and R. M. McMeeking, "Mechanical metamaterials at the theoretical limit of isotropic elastic stiffness," Nature **543**(7646), 533–537 (2017).

[6] F. Wang and O. Sigmund, "3D architected isotropic materials with tunable stiffness and buckling strength," J. Mech. Phys. Solids **152**, 104415 (2021).

[7] J. L. Silverberg, A. A. Evans, L. McLeod, R. C. Hayward, T. Hull, C. D. Santangelo, and I. Cohen, "Using origami design principles to fold reprogrammable mechanical metamaterials," Science **345**(6197), 647–650 (2014).

[8] S. Shan, S. H. Kang, J. R. Raney, P. Wang, L. Fang, F. Candido, J. A. Lewis, and K. Bertoldi, "Multistable architected materials for trapping elastic strain energy," Adv. Mater. **27**(29), 4296–4301 (2015).

[9] T. Frenzel, C. Findeisen, M. Kadic, P. Gumbsch, and M. Wegener, "Tailored buckling microlattices as reusable light-weight shock absorbers," Adv. Mater. **28**(28), 5865–5870 (2016).

[10] R. Lakes, "Materials with structural hierarchy," Nature **361**(6412), 511–515 (1993).

[11] L. R. Meza, S. Das, and J. R. Greer, "Strong, lightweight, and recoverable three-dimensional ceramic nanolattices," Science **345**(6202), 1322–1326 (2014).

[12] L. R. Meza, A. J. Zelhofer, N. Clarke, A. J. Mateos, D. M. Kochmann, and J. R. Greer, "Resilient 3D hierarchical architected metamaterials," Proc. Natl. Acad. Sci. U. S. A. **112**(37), 11502–11507 (2015).

[13] R. Lakes, "Deformation mechanisms in negative Poisson ratio materials: Structural aspects," J. Mater. Sci. **26**(9), 2287–2292 (1991).

[14] S. Babaee, J. Shim, J. C. Weaver, E. R. Chen, N. Patel, and K. Bertoldi, "3D soft metamaterials with negative Poisson's ratio," Adv. Mater. **25**(36), 5044–5049 (2013).

[15] F. Wang, O. Sigmund, and J. S. Jensen, "Design of materials with prescribed nonlinear properties," J. Mech. Phys. Solids **69**, 156–174 (2014).

[16] F. Wang, "Systematic design of 3D auxetic lattice materials with programmable Poisson's ratio for finite strains," J. Mech. Phys. Solids **114**, 303–318 (2018).

[17] A. Rafsanjani, A. Akbarzadeh, and D. Pasini, "Snapping mechanical metamaterials under tension," Adv. Mater. **27**(39), 5931–5935 (2015).

[18] K.-I. Jang, H. U. Chung, S. Xu, C. H. Lee, H. Luan, J. Jeong, H. Cheng, G.-T. Kim, S. Y. Han, J. W. Lee, J. Kim, M. Cho, F. Miao, Y. Yang, H. N. Jung, M. Flavin, H. Liu, G. W. Kong, K. J. Yu, S. I. Rhee, J. Chung, B. Kim, J. W. Kwak, M. H. Yun, J. Y. Kim, Y. M. Song, U. Paik, Y. Zhang, Y. Huang, and J. A. Rogers, "Soft network composite materials with deterministic and bio-inspired designs," Nat. Commun. **6**(1), 6566 (2015).

[19] D. M. Kochmann and K. Bertoldi, "Exploiting microstructural instabilities in solids and structures: From metamaterials to structural transitions," Appl. Mech. Rev. **69**(5), 050801 (2017).

[20] M. M. Neves, O. Sigmund, and M. P. Bendsøe, "Topology optimization of periodic microstructures with buckling criteria," in Proceedings of the Fifth World Congress on Computational Mechanics, 2002.

[21] C. R. Thomsen, F. Wang, and O. Sigmund, "Buckling strength topology optimization of 2D periodic materials based on linearized bifurcation analysis," Comput. Methods Appl. Mech. Eng. **339**, 115–136 (2018).

[22] G. L. Bluhm, O. Sigmund, F. Wang, and K. Poulios, "Nonlinear compressive stability of hyperelastic 2D lattices at finite volume fractions," J. Mech. Phys. Solids **137**, 103851 (2020).

[23]F. Wang and O. Sigmund, "Numerical investigation of stiffness and buckling response of simple and optimized infill structures," Struct. Multidiscip. Optim. **61**(6), 2629–2639 (2020).
[24]F. Wang, B. S. Lazarov, and O. Sigmund, "On projection methods, convergence and robust formulations in topology optimization," Struct. Multidiscip. Optim. **43**(6), 767–784 (2011).
[25]R. S. Rivlin, "Large elastic deformations of isotropic materials. IV. Further developments of the general theory," Philos. Trans. R. Soc. London, Ser. A **241**(835), 379–397 (1948).
[26]Y. Renard and K. Poulios, "GetFEM: Automated FE modeling of multiphysics problems based on a generic weak form language," ACM Trans. Math. Software **47**(1), 1 (2020).
[27]C. Geuzaine and J.-F. Remacle, "Gmsh: A 3-D finite element mesh generator with built-in pre- and post-processing facilities," Int. J. Numer. Methods Eng. **79**(11), 1309–1331 (2009).
[28]R. De Pascalis, M. Destrade, and A. Goriely, "Nonlinear correction to the Euler buckling formula for compressed cylinders with guided-guided end conditions," J. Elasticity **102**(2), 191–200 (2011).